Available online at www.sciencedirect.com
ScienceDirect
Planetary and Space Science 55 (2007) 1990–2009
Planetary and Space Science
www.elsevier.com/locate/pss

Near-surface winds at the Huygens site on Titan: Interpretation by means of a general circulation model

Tetsuya Tokano*

Institut für Geophysik und Meteorologie, Universität zu Köln, Albertus-Magnus-Platz, 50923 Köln, Germany

Accepted 13 April 2007
Available online 25 April 2007

Abstract

This study aims at interpreting the zonal and meridional wind in Titan's troposphere measured by the Huygens probe by means of a general circulation model. The numerical simulation elucidates the relative importance of the seasonal variation in the Hadley circulation and Saturn's gravitational tide in affecting the actual wind profile. The observed reversal of the zonal wind at two altitudes in the lower troposphere can be reproduced with this model only if the near-surface temperature profile is asymmetric about the equator and substantial seasonal redistribution of angular momentum by the variable Hadley circulation takes place. The meridional wind near the surface is mainly caused by the meridional pressure gradient and is thus a manifestation of the Hadley circulation. Southward meridional wind in the PBL (planetary boundary layer) is consistent with the near-surface temperature at the equator being lower than at mid southern latitudes. Even small changes in the radiative heating profile in the troposphere can substantially affect the mean zonal and meridional wind including their direction. Saturn's gravitational tide is rather weak at the Huygens site due to the proximity to the equator, and does not clearly manifest itself in the instantaneous vertical profile of wind. Nevertheless, the simulated descent trajectory is more consistent with the observation if the tide is present. Because of a different force balance in Titan's atmosphere from terrestrial conditions, PBL-specific wind systems like on Earth are unlikely to exist on Titan.

Keywords: Titan; Meteorology; Wind; Huygens

1. Introduction

For many years the research of the atmospheric dynamics of Saturn's moon Titan has focussed on the stratospheric superrotation and its formation mechanisms. On the other hand, our knowledge of the atmospheric circulation in Titan's troposphere was poor or nearly absent prior to the Cassini/Huygens mission. The relevance of near-surface winds for Titan's geology is evident from recently detected aeolian features such as longitudinal sand dunes (Lorenz et al., 2006) and other putative wind streaks (Porco et al., 2005). Moreover, the near-surface wind may be regarded as an important component in the atmospheric angular momentum cycle (Tokano and Neubauer, 2005). General circulation models (GCMs) of Titan's atmosphere predicted wind speeds of a few $m\,s^{-1}$ up to some tens of $m\,s^{-1}$ in the troposphere. However, there are substantial differences in the predicted wind speeds among models (Hourdin et al., 1995; Tokano et al., 2001; Tokano and Neubauer, 2002; Rannou et al., 2004; Tokano and Neubauer, 2005). Shortly before the arrival of Cassini/Huygens at Titan, astronomical observations of tropospheric clouds at high southern latitudes began providing the first data on the wind speed and direction at least at those locations where clouds appeared (Bouchez and Brown, 2005; Roe et al., 2005; Schaller et al., 2006). In most cases weak eastward wind was retrieved, but sometimes also northward drift was observed (Roe et al., 2005). However, since convective clouds develop only at altitudes higher than 10 km (Griffith et al., 2005), the cloud drift speed may not be representative of near-surface winds. The Huygens probe that descended into Titan's atmosphere on 14 January 2005 provided the first in situ data of wind speed and direction in Titan's troposphere, as described in Section 2.

*Tel.: +49 221 4704489; fax: +49 221 4705198.
E-mail address: tokano@geo.uni-koeln.de.

0032-0633/$ - see front matter © 2007 Elsevier Ltd. All rights reserved.
doi:10.1016/j.pss.2007.04.011

The purpose of this study is twofold. First, it aims at understanding the wind system in the lower troposphere of Titan. Particularly it is investigated to what extent Earth-like meteorology can be expected on Titan. The second purpose is to verify the GCM prediction concerning the tropospheric wind data. Such a verification was not possible prior to the Huygens mission. Section 2 summarises the wind data in Titan's troposphere obtained from Huygens. In Section 3 the observed wind profile is analytically analysed, taking into account various characteristic wind systems known in the terrestrial atmospheric boundary layer. Section 4 presents a set of numerical simulations under various assumptions in an effort to reproduce and interpret the observed wind profile. The GCM is run under different assumptions concerning the global atmospheric circulation such as presence or absence of Saturn's gravitational tide, i.e. the force that arises on Titan due to the elliptical orbit of Titan (Tokano and Neubauer, 2002), and seasonal effects (Tokano, 2005). In Section 5 the descent trajectory of the Huygens probe is simulated with the wind profile predicted by the GCM and compared with observation. The overall results are discussed in general context in Section 6.

2. Near-surface wind data acquired by Huygens

The Doppler Wind Experiment (DWE) onboard the Huygens probe performed a precise in situ measurement of the wind speed in Titan's atmosphere from an altitude of 146 km down to the surface (Bird et al., 2005; Folkner et al., 2006). The wind profile in the lower troposphere is depicted in Fig. 7 of Folkner et al. (2006). The DWE wind is slightly eastward near the surface below 1 km, turns to westward between 1 and 5 km and then returns to zero by 5 km. The wind profile between 5 and 13 km is unknown, but is likely to be prograde and to increase to $3\,m\,s^{-1}$ at 13 km, above which the wind speed smoothly increases with altitude. In this data retrieval the meridional wind was assumed to be zero. Due to the ambiguity of the zonal and meridional drift direction of Huygens the same Doppler shift could in principle be generated by several combinations of u and v. For instance eastward wind of $1\,m\,s^{-1}$ has a projection in the direction to Earth of $-0.505\,m\,s^{-1}$ and a northward wind of $1\,m\,s^{-1}$ has a projection in the direction to Earth of $0.239\,m\,s^{-1}$ (Folkner et al., 2006). In other words it is also possible to interpret the eastward wind of $1\,m\,s^{-1}$ as southward wind of $-2.11\,m\,s^{-1}$.

Horizontal wind speed and direction were also retrieved from ground tracking of the Huygens probe by the DISR (Descent Imager Spectral Radiometer) (Tomasko et al., 2005; Karkoschka et al., 2007). The probe initially drifted eastward with a slight additional southward drift down to an altitude of 7 km. It then quickly turned and drifted westnorthwestward with a speed of $\sim 1\,m\,s^{-1}$ down to 800 m at which a second left turn took place. Eventually the probe approached the surface with less than $0.3\,m\,s^{-1}$ towards southeast or southsoutheast. The meridional wind was southward from the upper troposphere down to 15 km, northward between 15 km and 800 m and southward in the lowest 800 m. Thus the wind vector performs nearly one complete albeit discontinuous rotation in the lower 7 km.

The lower part of the troposphere comprises the planetary boundary layer (PBL), which represents a transitional layer between the planetary surface and atmosphere in which the atmospheric dynamics is substantially affected by the surface. The characteristics of Titan's PBL were described based on the thermal structure retrieved by the Huygens Atmospheric Structure Instrument (HASI) (Tokano et al., 2006). The PBL at the Huygens site was weakly convective and had an approximate depth of 300 m, with presumably negligible diurnal variation. The mean wind speed in the surface layer within the PBL comprising the lowest 10 m was estimated to be $0.04\,m\,s^{-1}$ or less based on the thermal profile in the PBL. On the other hand, the wind profile above 10 m could not be estimated from these data. Also the thermal behaviour of the Huygens probe after the landing on Titan indicated that the near-surface winds were less than $0.2\,m\,s^{-1}$, and probably much less (Lorenz, 2006).

While some tentative explanations for the observed wind profile near the surface have already been given (Bird et al., 2005; Tomasko et al., 2005; Folkner et al., 2006), we are left with several questions that can be formulated as follows:

1. Why is there a multiple reversal of both the zonal and meridional wind near the surface?
2. Why is the meridional wind near the surface faster than a few kilometres above? Is there evidence of Saturn's gravitational tide or Hadley circulation?
3. What is the likely temporal and spatial variation of the wind profile?
4. Is the Huygens wind profile representative of whole Titan?

3. Analytic interpretation of the observed wind profile

Three basic types of wind profile are known to exist in the terrestrial PBL (e.g. Stull, 1988). The wind profile characteristic of a PBL with neutral thermal stratification is the Ekman spiral although a pure Ekman spiral is rarely observed. On the other hand, the wind speed in a convective PBL (with an unstable stratification) is roughly uniform across the PBL outside the surface layer by virtue of intense vertical mixing. The third type is the nocturnal, stable PBL characterised by a large vertical variation in wind speed within the PBL, with a marked peak (low-level jet) near the top of the PBL. Each of these characteristic wind profiles occurs under idealised (homogeneous, stationary, dry, etc.) conditions, so the wind can further be affected by inhomogeneous, non-stationary conditions.

3.1. Ekman spiral

We first consider whether the observed wind profile may represent an Ekman spiral under neutrally stratified condition. In an Ekman spiral the wind speed decreases from the geostrophic wind in the free atmosphere to zero at the surface and the wind vector describes a spiral because of the variation in wind direction with altitude. This spiral is a result of the variation with height of the zonal and meridional Coriolis force within the PBL.

Evident to the eyes is the fact that the shape of the descent trajectory reconstructed by Karkoschka et al. (2007) is not characteristic of an Ekman spiral in that the total turn angle of ~315° is by far too large to be consistent with an Ekman spiral and the wind turn occurs in two sharp reversals rather than in a smooth loop.

A more precise assessment is possible if one constructs a hypothetical Ekman spiral that is consistent with the PBL parameters derived by Tokano et al. (2006). An analytic solution of the zonal and meridional wind, u and v, in the Ekman spiral (e.g. Stull, 1988) can be written as

$$u = u_g[1 - \exp(-z/D)\cos(z/D)], \quad (1)$$

$$v = -u_g \exp(-z/D)\sin(z/D), \quad (2)$$

where u_g is the geostrophic wind speed, z is the altitude and D is the depth of an Ekman spiral. Here the negative sign of the right-hand side of Eq. (2) stands for the southern hemisphere in which the Huygens site is located (in the northern hemisphere the sign is positive).

Here,

$$D = \sqrt{\frac{2K}{f}}, \quad (3)$$

where $K = 7.4 \times 10^{-3}\,\mathrm{m^2\,s^{-1}}$ is the eddy diffusivity at the Huygens site adopted from Tokano et al. (2006) and $f = 1.63 \times 10^{-6}\,\mathrm{s^{-1}}$ is the Coriolis parameter at the Huygens site.

The major unknown in these equations is the geostrophic wind u_g that cannot be calculated because the meridional pressure gradient at the Huygens site is unknown from observations. Particularly it is unknown whether u_g is positive or negative. Therefore, we assume that $u_g = \pm 1\,\mathrm{m\,s^{-1}}$ because this is close to the zonal wind observed by Huygens near 300 m.

Fig. 1 shows the analytic vertical profile of an Ekman spiral calculated with Eqs. (1) and (2) for positive (eastward, prograde) and negative (westward, retrograde) values of u_g. In either case the wind vector spirals anticlockwise with increasing altitude, as the Huygens site is located in the southern hemisphere. If the geostrophic wind is positive ($+1\,\mathrm{m\,s^{-1}}$, eastward), the zonal wind in the Ekman spiral increases rapidly with altitude within the lowest 200 m, slightly exceeds the geostrophic speed near 200 m and then stays nearly constant at $1\,\mathrm{m\,s^{-1}}$ at higher altitudes. At the same time the meridional wind increases from zero to $0.3\,\mathrm{m\,s^{-1}}$ (northward) at 75 m and then returns to zero by 300 m, the top of the PBL. Meridional wind in the free atmosphere is negligible. This wind profile is consistent with the DWE data only in the lowest 300 m, i.e. within the PBL. The reversal of the zonal wind direction near 1 km is not consistent with the Ekman spiral and since the actual zonal wind substantially deviates from $1\,\mathrm{m\,s^{-1}}$, this cannot be regarded as geostrophic wind.

If we instead assume $u_g = -1\,\mathrm{m\,s^{-1}}$, both the zonal and meridional wind of the Ekman spiral exhibit a reversed vertical profile. Although this zonal wind agrees better with the observed wind speed and direction above 1 km, there is

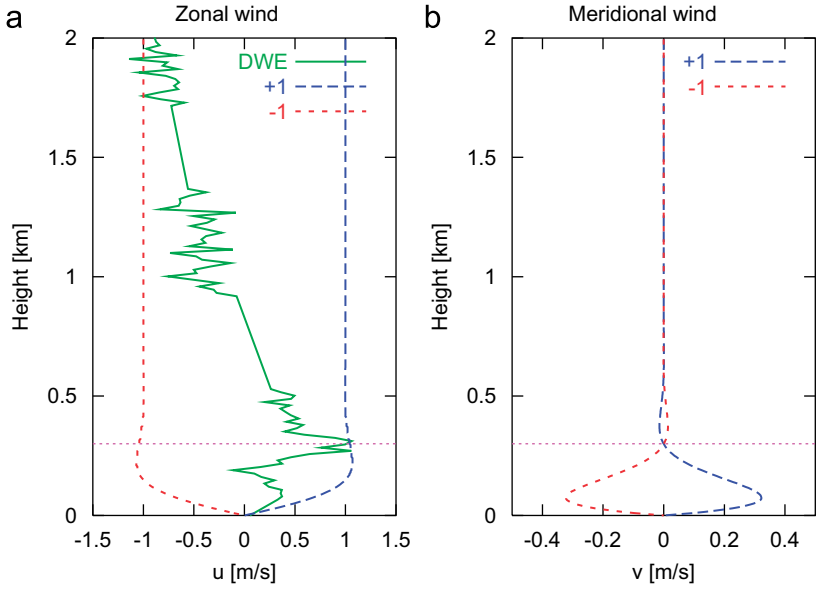

Fig. 1. Hypothetical Ekman spiral in Titan's PBL at the Huygens site for different geostrophic winds ($\pm 1\,\mathrm{m\,s^{-1}}$). Positive zonal wind is eastward and positive meridional wind is northward. Also displayed for comparison is the zonal wind measured by the Huygens DWE (Folkner et al., 2006) adopted from the ESA-Huygens Data Archive. The thin horizontal line at 0.3 km marks the top of the PBL as inferred by Tokano et al. (2006).

a large discrepancy below 1 km in that the eastward wind near the surface is impossible in an Ekman spiral with a westward geostrophic wind. A similar statement can be made concerning the meridional wind. Neither a prograde nor retrograde geostrophic wind can generate the observed simultaneous presence of northerly and southerly wind in the PBL.

In this consideration it was assumed that, according to Bird et al. (2005) and Folkner et al. (2006), the meridional component of the observed wind profile is negligible. If we now hypothetically drop this assumption and consider the most extreme opposite assumption, i.e. that the DWE data arose solely from meridional wind and that the zonal wind was negligible, this would require a peak southward wind of about $-2\,\mathrm{m\,s^{-1}}$ near 300 m and an increase of the northward wind speed above 1 km altitude. Such a wind profile is even more inconsistent with an Ekman spiral, as can be readily seen from Fig. 1b for $u_g \pm 1\,\mathrm{m\,s^{-1}}$.

This means that an Ekman spiral cannot qualitatively reproduce the vertical profile of zonal wind in the lowest few kilometres observed by the Huygens DWE irrespective of the sign of geostrophic wind. The steepness of the Ekman spiral at a given site is sensitive to the eddy diffusivity and a larger eddy diffusivity than retrieved by Tokano et al. (2006) would deepen the Ekman spiral, but still the reversal of the zonal wind direction cannot be generated in an Earth-like Ekman spiral.

3.2. Further simplified wind profiles

Tokano et al. (2006) identified that the PBL at the Huygens site is weakly convective and has a depth of 300 m. In a strongly convective PBL the wind speed in the outer layer of the PBL tends to be uniform by virtue of vertical mixing (Stull, 1988). However, the observed wind profile is certainly not uniform within the PBL (and also beyond the PBL). Instead the wind speed varies between 0 and $\sim 1\,\mathrm{m\,s^{-1}}$ within the lowest kilometre (Folkner et al., 2006). This inconsistency suggests that the vertical mixing of momentum in the PBL is by far too weak to maintain a wind speed which is constant with height, as is evident from a tiny eddy diffusivity of $7.4 \times 10^{-3}\,\mathrm{m^2\,s^{-1}}$ (Tokano et al., 2006).

At a glance the local maximum of wind speed near 300 m (Folkner et al., 2006) is also suggestive of a low-level jet characteristic of a stably stratified, nocturnal PBL. However, there are several reasons to discard the likelihood of a low-level jet mechanism. Low-level jets in a nocturnal PBL are usually caused by inertial oscillations. This develops if the PBL becomes decoupled from the surface because of weak turbulence and if there is no horizontal pressure gradient (Stull, 1988). Under this condition the Coriolis force is no longer balanced by the pressure gradient force and turbulence, so the wind begins to accelerate and to rotate with a period of $2\pi/f$, where f is the Coriolis parameter.

In the case of Titan the Coriolis force is unlikely to be unbalanced at any instance. Fig. 2 shows a comparison of several meridional forces at the Huygens site as a function of altitude. The meridional Coriolis force, $-fu$, scales with the wind speed measured by DWE (Folkner et al., 2006), and varies between -4×10^{-6} and $2 \times 10^{-6}\,\mathrm{m\,s^{-2}}$ in the lower 5 km. The centrifugal force, $-\tan\phi u^2/a$, where ϕ is the latitude and a is Titan's radius, is northward, but negligible in this altitude region. The meridional component of Saturn's tide calculated after Tokano and Neubauer (2002) for the time and place of Huygens landing is $2.3 \times 10^{-6}\,\mathrm{m\,s^{-2}}$, i.e. northward. Thus the tide has a magnitude comparable with the Coriolis force. The presence of a substantial force other than the Coriolis force means that the most important prerequisite (unbalanced Coriolis force) is not satisfied. Therefore, the local wind maximum near 300 m should not be regarded as an Earth-like low-level jet characteristic of a nocturnal PBL.

We can conclude that the near-surface wind profile observed by Huygens cannot be simply understood by

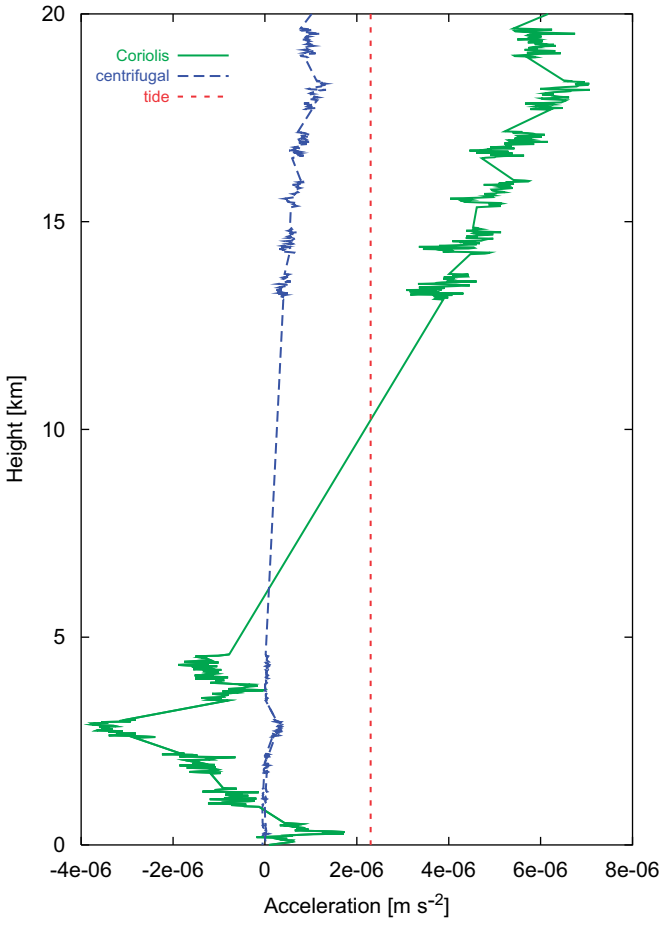

Fig. 2. Comparison of three major forces in meridional direction at the Huygens site. The Coriolis and centrifugal force are calculated with the zonal wind after Folkner et al. (2006) and Saturn's instantaneous gravitational tide is calculated after Tokano and Neubauer (2002). No wind data could be retrieved for altitudes between 5 and 13 km by DWE (Folkner et al., 2006), so the Coriolis and centrifugal force are linearly interpolated. Positive acceleration is northward.

PBL-specific wind systems known in terrestrial boundary layer meteorology under any thermal stratification. This implies that the influence of horizontal inhomogeneity in the surface or atmospheric properties as well as large-scale atmospheric dynamics have to be taken into account. Therefore, we investigate in the next section the actual wind profile at the Huygens site in the context of global-scale atmospheric dynamics.

4. Interpretation by means of a GCM

4.1. Baseline simulation (Simulation 1)

As a next step we make use of a three-dimensional Titan GCM to understand the wind profile measured by Huygens. The main purpose of such simulations is to put the instantaneous single wind profile into the context of global-scale atmospheric circulation considering various effects that may play a role such as Saturn's gravitational tide, Hadley circulation and seasonal variation. For this study the GCM of Tokano and Neubauer (2005) is applied that is described in that paper and preceding papers of the group (Tokano et al., 1999; Tokano and Neubauer, 2002; Tokano, 2005). The radiation code is that of McKay et al. (1989). The methane mixing ratio for the calculation of the radiative fluxes is prescribed as a sole function of altitude after Lellouch et al. (1989). The methane cycle (condensation and transport) is not predicted unlike in Tokano et al. (2001) or Rannou et al. (2006). Similarly the vertical profile of the haze and stratospheric gases is held fixed after McKay et al. (1989). The ground surface temperature is predicted assuming thermal properties of porous icy regolith (surface type 1) as described in Tokano (2005). The bulk soil density is $\rho = 800\,\mathrm{kg\,m^{-3}}$, the soil thermal conductivity is $\kappa = 0.1\,\mathrm{W\,m^{-1}\,K^{-1}}$, the soil-specific heat capacity is $c = 1400\,\mathrm{J\,K^{-1}\,kg^{-1}}$, resulting in a surface thermal inertia of $I = 334.7\,\mathrm{J\,m^{-2}\,s^{-1/2}\,K^{-1}}$. The surface albedo is $A = 0.38$, the surface emissivity is $\varepsilon = 0.86$ and the surface drag coefficient is $C_D = 0.002$. Saturn's gravitational tide is calculated after Tokano and Neubauer (2002).

The assumed atmospheric and surface parameters are not updated with information gathered from the Huygens mission since many relevant data have not yet been published and it makes little sense to update only those parameters already published, such as surface albedo and column optical depth of the haze (Tomasko et al., 2005) or vertical profile of methane mixing ratio (Niemann et al., 2005). Also no attempt is made to include global topography or spatial variation in surface albedo or thermal inertia since global maps of surface parameters that can readily be incorporated into climate models do not yet exist for Titan and this is a separate topic beyond the scope of this work.

The baseline simulation (Simulation 1, see Table 1 for an overview of GCM simulations) includes Saturn's tide and includes the seasonal cycle of insolation.

Table 1
Overview of the GCM versions run in this study

Simulation no.	Tide	Seasonality	Solar heating
1	Yes	Yes	Nominal
2	No	Yes	Nominal
3	Yes	No	Nominal
4	Yes	Yes	Reduced

4.1.1. Zonal wind

In Tokano and Neubauer (2005) it was shown that the zonal wind in the lower troposphere undergoes substantial seasonal variation as a result of latitudinal and vertical redistribution of atmospheric angular momentum by virtue of the Hadley circulation and surface friction.

Fig. 3 shows the meridional–vertical cross-section of the zonally and diurnally averaged zonal wind u at different seasons. The seasonal variation in u can only be meaningfully understood in combination with the global temperature field depicted in Fig. 4. The main driver of the changing wind field is the insolation that heats up the surface. The solar radiation gives rise to a pole-to-pole surface temperature gradient (Fig. 1 of Tokano, 2005). Subsequently, the PBL in the summer hemisphere is heated by virtue of sensible heat flux from the warm surface, causing a warm summer pole and a cold winter pole, with a decreasing latitudinal temperature contrast with increasing height (Fig. 4). The simulation also illustrates that the latitudinal temperature gradient is predicted to reverse quickly when the Sun crosses the equator at equinox.

The zonal wind field is tightly correlated with the solar forcing, as the Hadley circulation (thermally direct circulation) transports angular momentum vertically and meridionally. Within the lower troposphere the global profile of the zonal wind resembles that in the terrestrial stratosphere in that the summer hemisphere exhibits easterlies (retrograde wind), while in a large part of the winter hemisphere the wind is eastward (prograde), with the core of the prograde and retrograde jets being located at 5 km altitude. The maximum wind speed of the jets is $\pm 4\,\mathrm{m\,s^{-1}}$. The zonal wind field reverses after the equinox as with the temperature field. A more or less hemispherically symmetric wind field with mainly prograde wind is found only during a short period after the equinoxes.

Fig. 5a shows the vertical profile of the zonal wind at the Huygens landing site (10°S) at different seasons. The annual amplitude of the zonal wind is smaller than at higher latitudes. Seasonal variation is evident only in the lower troposphere below ~17 km. The reason for this is that under the predicted conditions the temperature variation occurs only up to that altitude (Fig. 4). At higher altitudes in the troposphere the thermal wind is virtually independent of season.

The vertical profile of zonal wind behaves like a string which is fixed at the surface and upper troposphere. The bulge of the string oscillates with a period of half a Titan

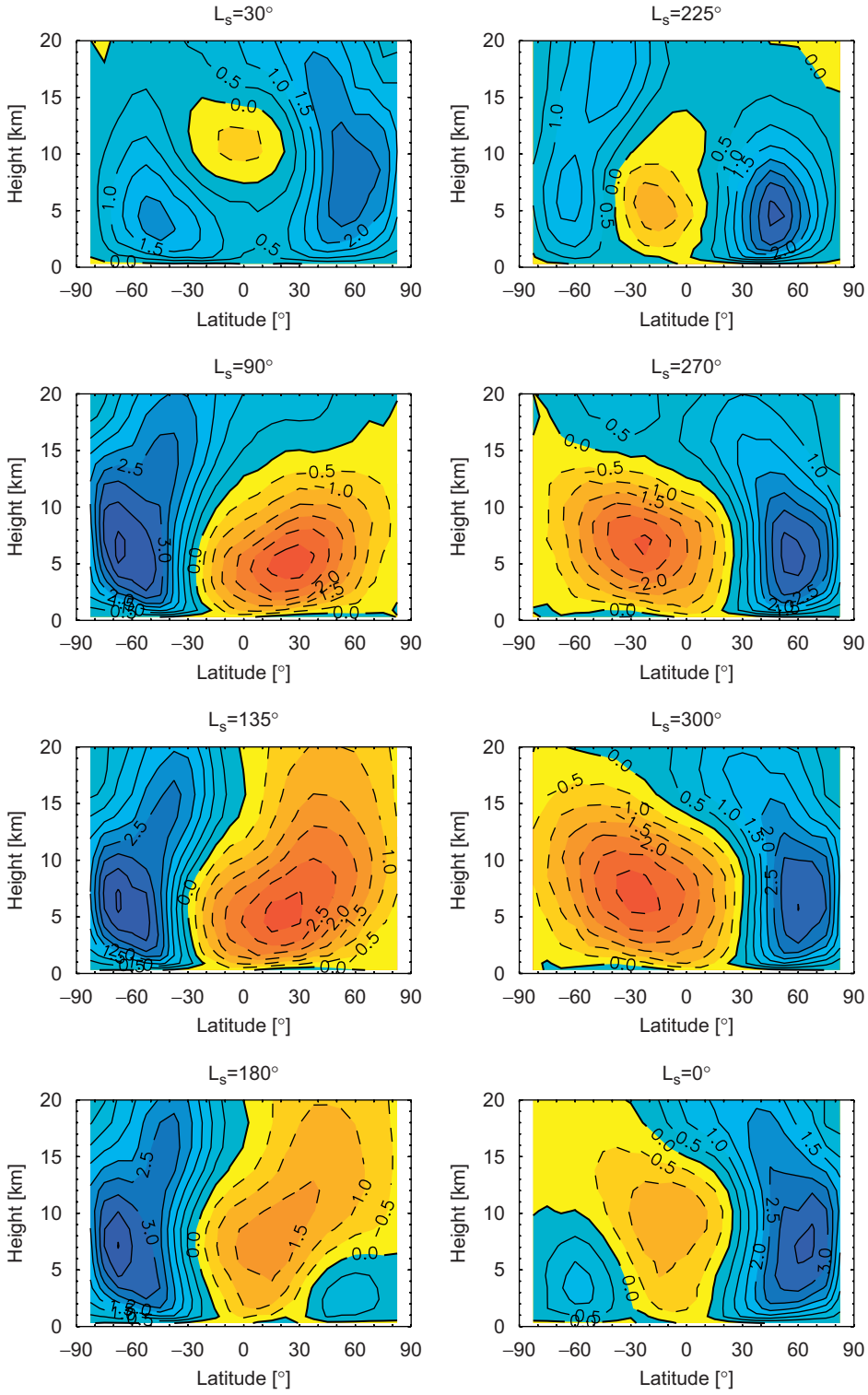

Fig. 3. Meridional–vertical cross-section of zonally and diurnally averaged zonal wind speed u (in m s^{-1}) in the lower troposphere predicted by the GCM (Simulation 1) at different seasons. Positive zonal wind is eastward (prograde) and is drawn with solid isotachs. L_S is the solar longitude describing the season (beginning with $L_S = 0^\circ$ at northern vernal equinox, see also Fig. 1 of Tokano et al., 1999). $L_S = 300^\circ$ is the season of Huygens descent.

year. The retrograde wind intensifies after each equinox and becomes fastest after the solstice. When the season approaches the next equinox, the retrograde wind weakens and the zonal wind near the surface turns to slightly prograde. This behaviour is characteristic of the equatorial region, in which the passage of the interface of two Hadley cells (intertropical convergence zone) occurs twice per Titan year near the equinoxes.

However, there is some difference between local summer and winter at the Huygens site. As can be seen from Fig. 3

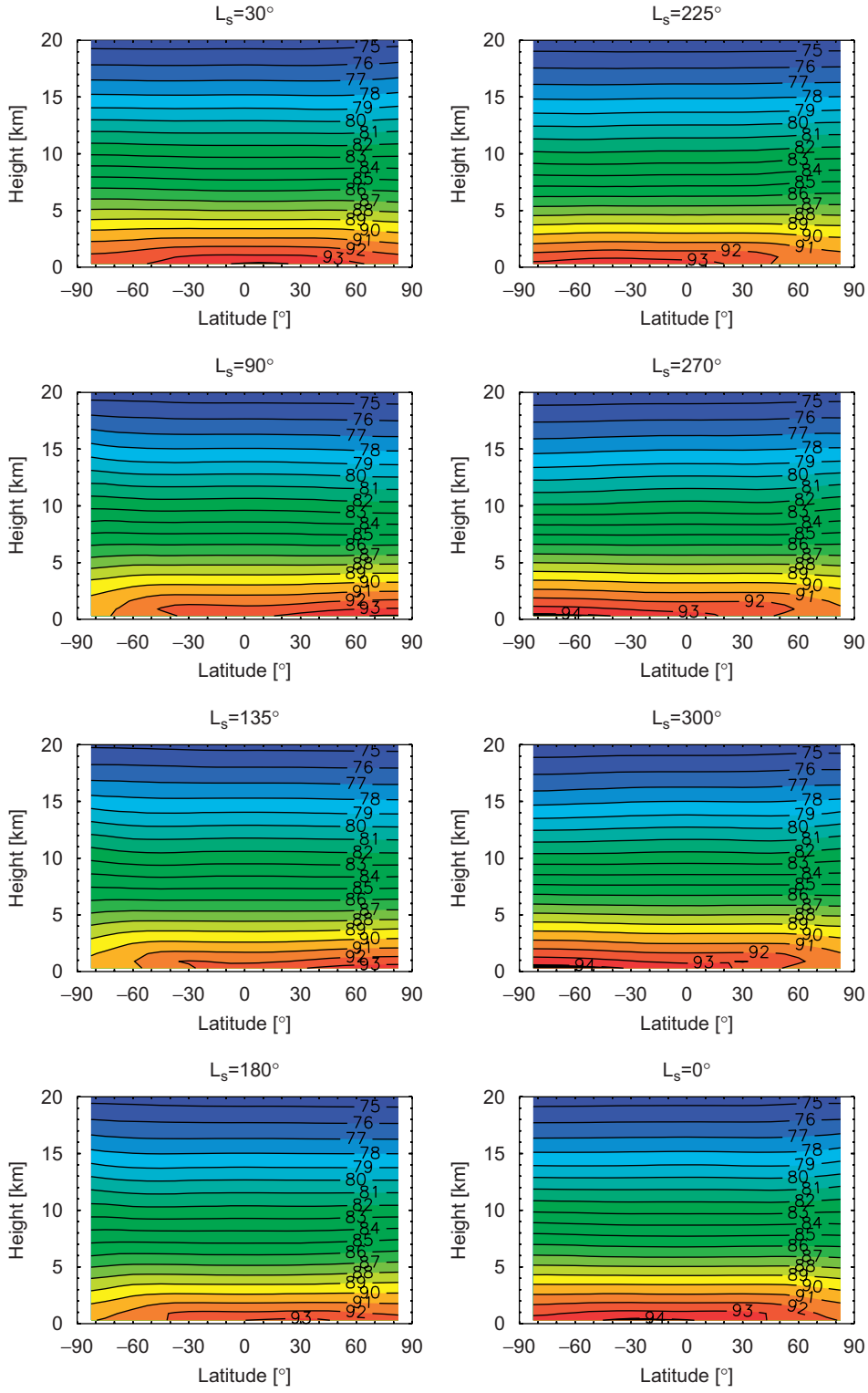

Fig. 4. Meridional–vertical cross-section of zonally and diurnally averaged temperature T (in K) in the lower troposphere predicted by the GCM (Simulation 1) at different seasons.

the Huygens site is located close to the boundary of easterlies and westerlies in southern winter ($L_S = 90°$), while it is close to the core of the easterlies in southern summer ($L_S = 300°$), the season of the Huygens descent. Therefore, the retrograde wind becomes fastest near the Huygens season.

Fig. 6a shows the instantaneous vertical profile of zonal wind predicted for the time and place of Huygens' landing along with the predictions of other scenarios discussed in the subsequent subsections. The zonal wind can readily be compared with the wind profile measured by the Huygens DWE (Folkner et al., 2006). The predicted zonal wind

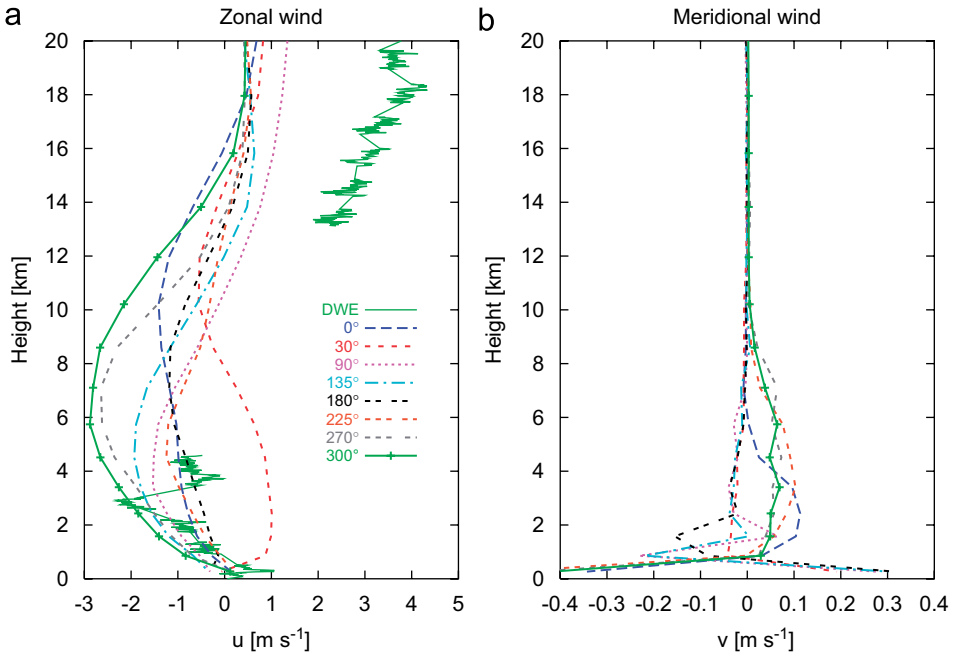

Fig. 5. Vertical profile of the diurnally averaged zonal wind (a) and meridional wind (b) at the Huygens site predicted by the GCM (baseline simulation) at different seasons (L_S). The DWE wind profile is shown for comparison as well.

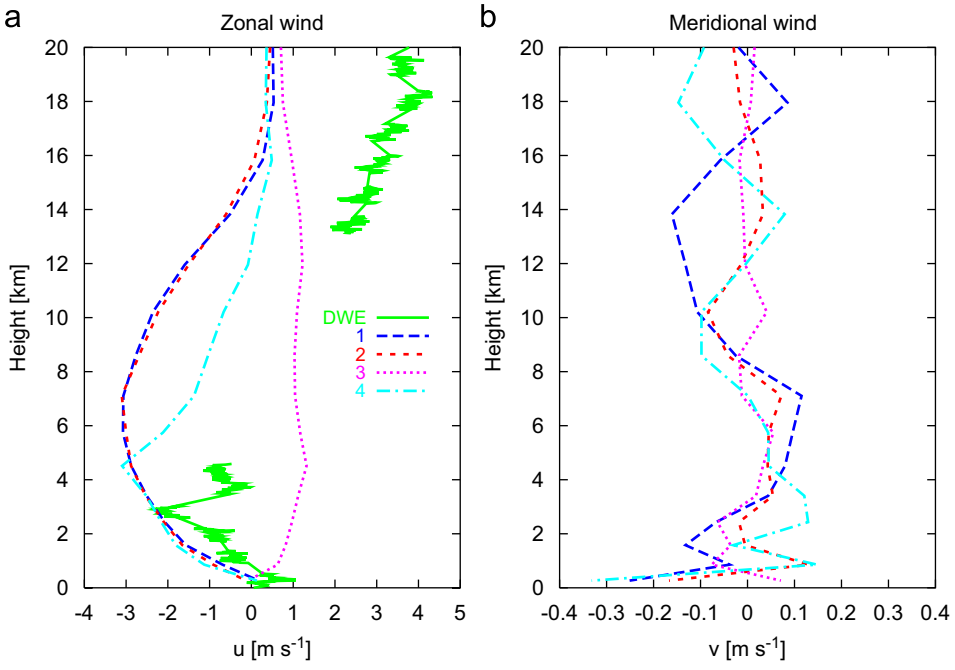

Fig. 6. Same as Fig. 5, but showing the instantaneous profile at the time and place of Huygens' landing. The numbers denote the simulation number explained in Table 1.

roughly agrees with the observed wind at altitudes below 3 km, except that the prograde wind below 1 km may be slightly too weak. Particularly, the reversal of the wind direction at 800 m and an increase of the retrograde wind in the lowest 3 km are nicely reproduced. On the other hand, the predicted wind has a peak retrograde wind near 7 km rather than at 3 km and the reversal from retrograde to prograde wind occurs near 15 km. Although there is a gap in the retrieved DWE data between 5 and 13 km (Folkner et al., 2006) it is reasonable to assume that this reversal takes place somewhere between 5 and 13 km, probably closer to 5 km. This quantitative discrepancy could indicate that in this model version the retrograde jet centred at southern mid latitudes is too strong. Possible cause of this is an excessive surface–atmosphere exchange of angular momentum, excessive seasonal variation in near-surface

temperature or seasonal lag in the solar forcing in the troposphere.

The predicted wind below 1 km is prograde although it seems to be weaker than measured by Huygens. However, as already mentioned in Section 2 there is some ambiguity between eastward and southward wind in the DWE data (Folkner et al., 2006). A part of the missing eastward wind in the predicted profile could be partly compensated by the near-surface southward wind. This aspect will be discussed in Section 5 in the context of the probe's descent trajectory.

The most obvious discrepancy between the GCM prediction and observation is the systematic underestimation of the prograde wind by about $3\,m\,s^{-1}$ at altitudes above 10 km (Figs. 5 and 6). In no season and no simulation run does the predicted wind speed approach the observed $3–4\,m\,s^{-1}$ near 20 km. This bias may be correlated with the inability of this GCM in generating strong stratospheric superrotation, as discussed in Tokano et al. (1999) or Tokano and Neubauer (2002), and is less likely to reflect inaccuracies in the predicted seasonal cycle. While this topic is beyond the scope of this study, possible discrepancies between the calculated and real radiative heating profile could be responsible for this discrepancy, as will be discussed in Section 4.4.

4.1.2. Meridional circulation and tide

One remarkable result of the Huygens mission was the detection of meridional winds in the troposphere down to the surface (Tomasko et al., 2005; Karkoschka et al., 2007). In this part of this study we elucidate the mechanism behind the observed meridional wind. Particularly, we investigate whether Saturn's gravitational tide, the Hadley circulation, transient eddies or something else can account for the observed meridional wind.

A persistent component of meridional circulation is the thermally direct circulation (Hadley circulation), which is present regardless of the gravitational tide. Fig. 7a depicts the mass streamfunction of the mean Hadley circulation in the Huygens season ($L_S = 300^\circ$) predicted by the GCM baseline version. As is typical of solstice-type circulation one single cell extends from the south pole to the north pole, except for a small opposite cell near the south pole. The streamlines indicate that southward flow exists below 2 km altitude at almost all latitudes, representing the lower branch of the Hadley cell. Upwelling occurs in the entire southern hemisphere, while downwelling occurs in the northern hemisphere.

Fig. 8 shows the instantaneous global map of temperatures at different levels in the atmosphere and at the surface. Also shown is the surface pressure at the time of Huygens' landing that is relevant in assessing the horizontal force balance as well as the relative role of tide and Hadley circulation. The subsolar point at the time of landing is located at 22°S, 208°E (152°W) close to the boundary between Shangri-La and Xanadu. The ground temperature peaks near 22°S, 220°E, i.e. 12° east of the subsolar point. At the Huygens site the ground temperature was 94.1 K, i.e. slightly warmer than the surface air (93.5 K) measured by HASI (Fulchignoni et al., 2005) and also warmer than predicted by the GCM for 300 m altitude (93.3 K). While the ground temperature undergoes a diurnal variation with an amplitude of ~1 K, the air temperature at 300 m is nearly independent of the solar local time, i.e. there is virtually no diurnal variation. Regions with a higher thermal inertia than assumed in the model will have even less diurnal variation, so the predicted longitudinal uniformity in the air temperature can be regarded as realistic. This is consistent with the conclusion of the analysis of the PBL by Tokano et al. (2006). Hence, unlike in the terrestrial PBL, it is unlikely that (thermally forced) diurnal variations in the PBL affect the wind profile.

Consequently, the global pattern of the surface pressure (Fig. 8d) does not correlate with the solar local time or pattern of the ground temperature. Instead the global surface pressure map exhibits a wave 2 pattern unique to the gravitational tide as described by Tokano and Neubauer (2002). At the time of Huygens landing two pressure maxima are found at the equator near 20°W and 160°E and two troughs are located in between, near 110°W and 70°E. These high pressures are regions of convergence of the tidal acceleration flow (Fig. 9a). In Tokano and Neubauer (2002) the surface pressure map was symmetric about the equator because in that model version seasonality was virtually absent owing to the temporally fixed ground surface temperature. In this simulation the longitudinally averaged surface pressure is higher at the north pole than at the south pole as a result of the pole-to-pole temperature gradient and the associated Hadley circulation. It turns out that the Huygens site is located just southeast of the centre of a tidally induced high-pressure region. Therefore, the pressure decreases from northwest to southeast at the Huygens site.

As a consequence of the tide, the horizontal pressure gradient undergoes a similar diurnal oscillation with a magnitude comparable to the tide (Fig. 10b). The surface pressure varies by ~1 hPa during a Titan day, and coincidentally attained a maximum at the time of Huygens descent (Fig. 10c). A comparison of Fig. 10a and b illustrates that the tide and pressure gradient are anti-correlated, i.e. there is an approximate balance between the tide and pressure gradient. This pressure gradient variation is clearly caused by the tide, and would disappear in its absence. The zonal pressure gradient has a larger amplitude than the meridional one, as with the tidal acceleration, but the diurnal average is zero. On the other hand, the diurnal average of the meridional pressure gradient is southward and is responsible for the cross-equatorial Hadley circulation. Wiggles superposed on the periodical oscillation of the pressure gradient force are caused by the finite response time of the pressure and wind field to adjust themselves to the changing tidal field.

However, it is also important to note that the tide at the Huygens site is weaker than at other locations. Fig. 10a

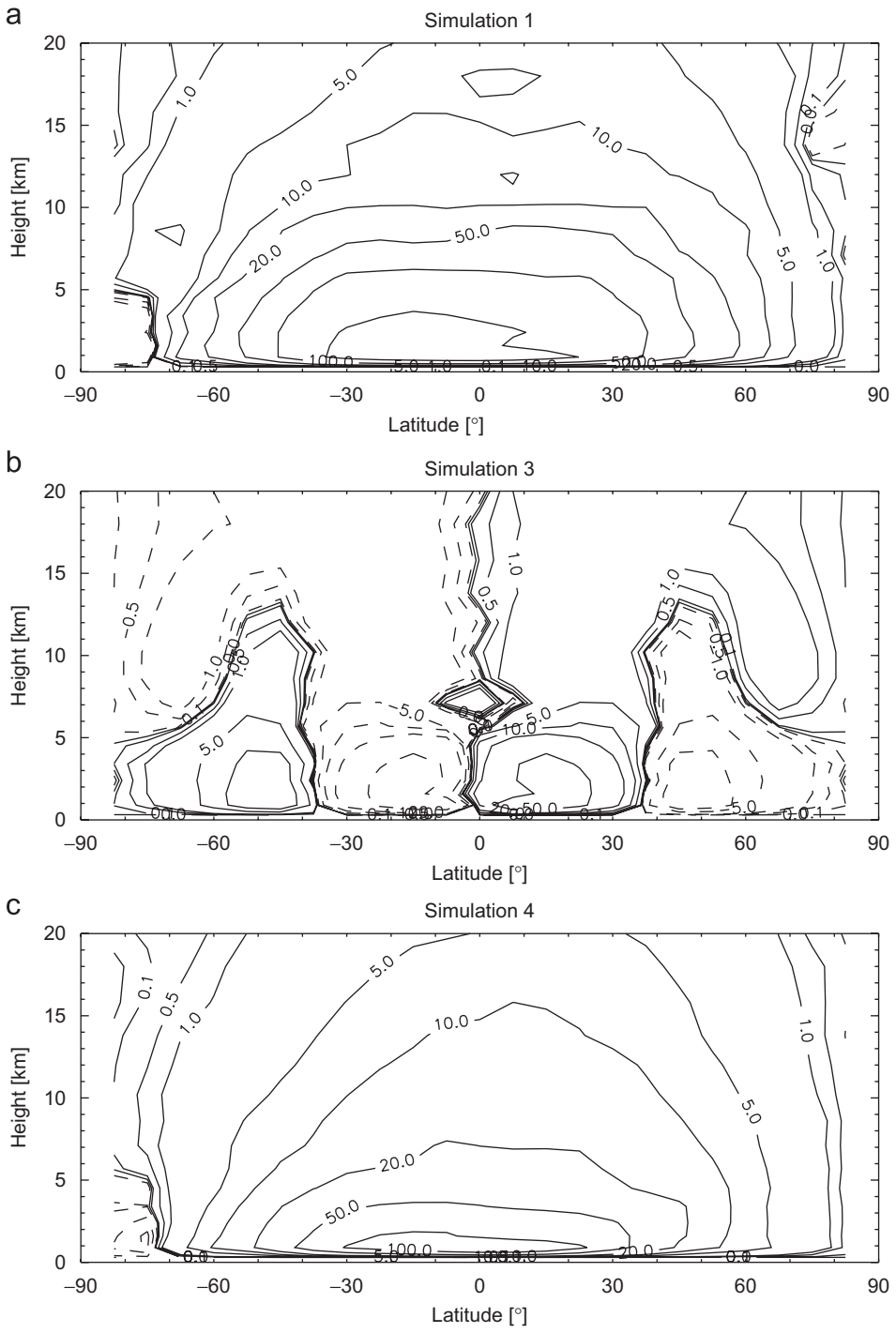

Fig. 7. Mass streamfunction (in 10^8 kg s^{-1}) of the Hadley circulation in the Huygens season predicted under three different conditions. The flow is clockwise/anti-clockwise along solid/dashed streamlines. The result for Simulation 2 is almost identical to that of Simulation 1, and thus is not shown.

illustrates that the meridional tide has an amplitude roughly three times weaker than the zonal tide. This behaviour is caused by the vicinity of the Huygens site to the equator, which is a symmetry axis of the tide where the meridional component vanishes for geometrical reasons. At the time of Huygens' landing the tide had a slight northward and a three times larger westward acceleration, so the tidal vector pointed westnorthwestward.

Fig. 9 shows the global map of the instantaneous horizontal wind vector at three levels in the troposphere (300, 4.5 and 20 km) along with the vector of Saturn's tidal acceleration. In no way does the wind vector follow the instantaneous direction of Saturn's gravitational tide. This is because the wind direction is a result of the horizontal force balance consisting, among others, of the pressure gradient force, tidal force and Coriolis force. The influence

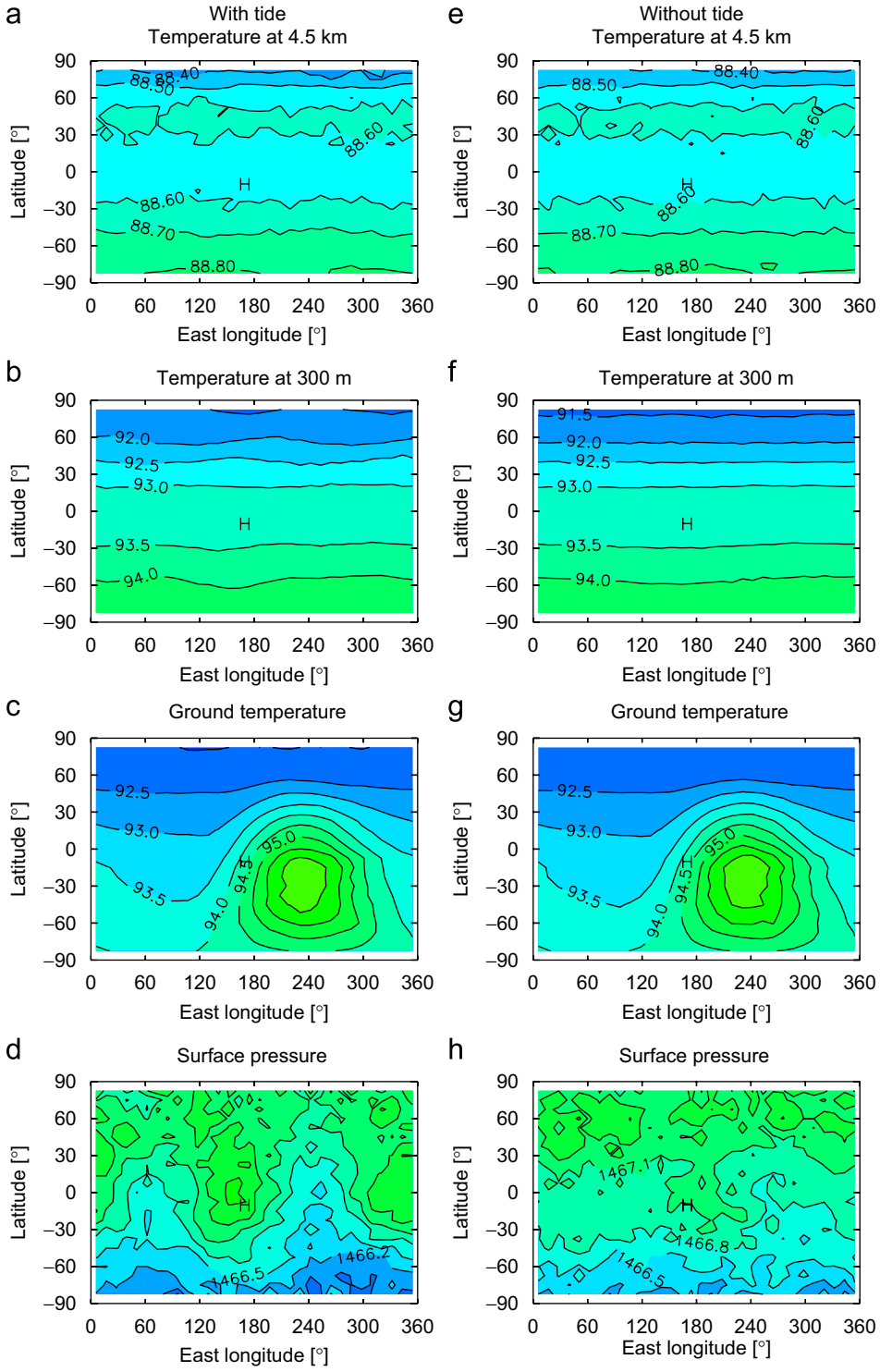

Fig. 8. Instantaneous global map of temperatures and surface pressure predicted by the GCM for the time of the Huygens descent. The left column shows the results with Saturn's tide (Simulation 1), the right column the results without Saturn's tide (Simulation 2). The temperatures are in K, the surface pressure in hPa. The Huygens site is marked as 'H'.

of the tide is best seen in the wave 2 pattern superposed on the main zonal flow.

However, it can also be seen that the tidally induced longitudinal variation in the meridional wind is rather weak near the equator including the Huygens site. The wind field at the top of the PBL (300 m) is more complex than at higher altitudes. At the Huygens site there is a generally southward cross-equatorial flow that is present at all longitudes. This cannot be ascribed to the tide, but to the strong southward pressure decrease (Fig. 8d). Since the Coriolis force disappears at the equator the southward pressure gradient force cannot be balanced by the Coriolis

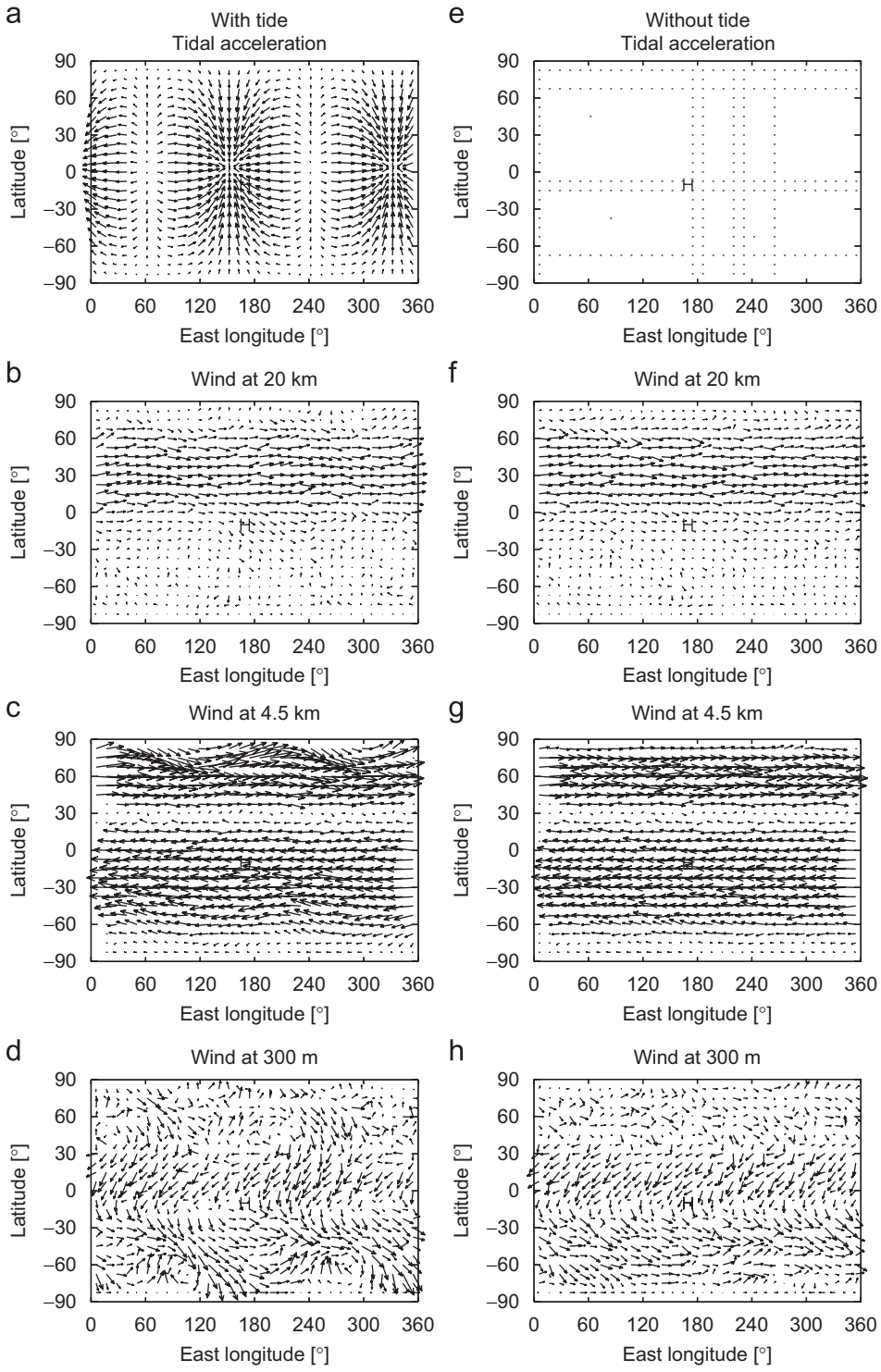

Fig. 9. Instantaneous global map of tidal acceleration and wind vector predicted by the GCM for the time of the Huygens descent. The tidal acceleration is defined in Tokano and Neubauer (2002). The wind vector length scales with the wind speed and one grid distance corresponds to $1\,m\,s^{-1}$ at 20 and 4.5 km altitude and $0.5\,m\,s^{-1}$ at 300 m.

force, as would be the case in a geostrophic balance, so the wind simply follows the pressure gradient. Thus it seems that the horizontal wind at the Huygens site is not substantially affected by Saturn's tide.

The diurnal-mean meridional wind v at the Huygens site is less than $0.01\,m\,s^{-1}$ in the upper troposphere above 10 km (Fig. 5b). It is faster near the surface, where it exceeds $0.3\,m\,s^{-1}$. v also exhibits a clear seasonal variation, although the annual amplitude is about 1 order of magnitude smaller than that of u. At the Huygens site the meridional wind direction reverses near 800 m altitude. Above 800 m northward wind is found in local

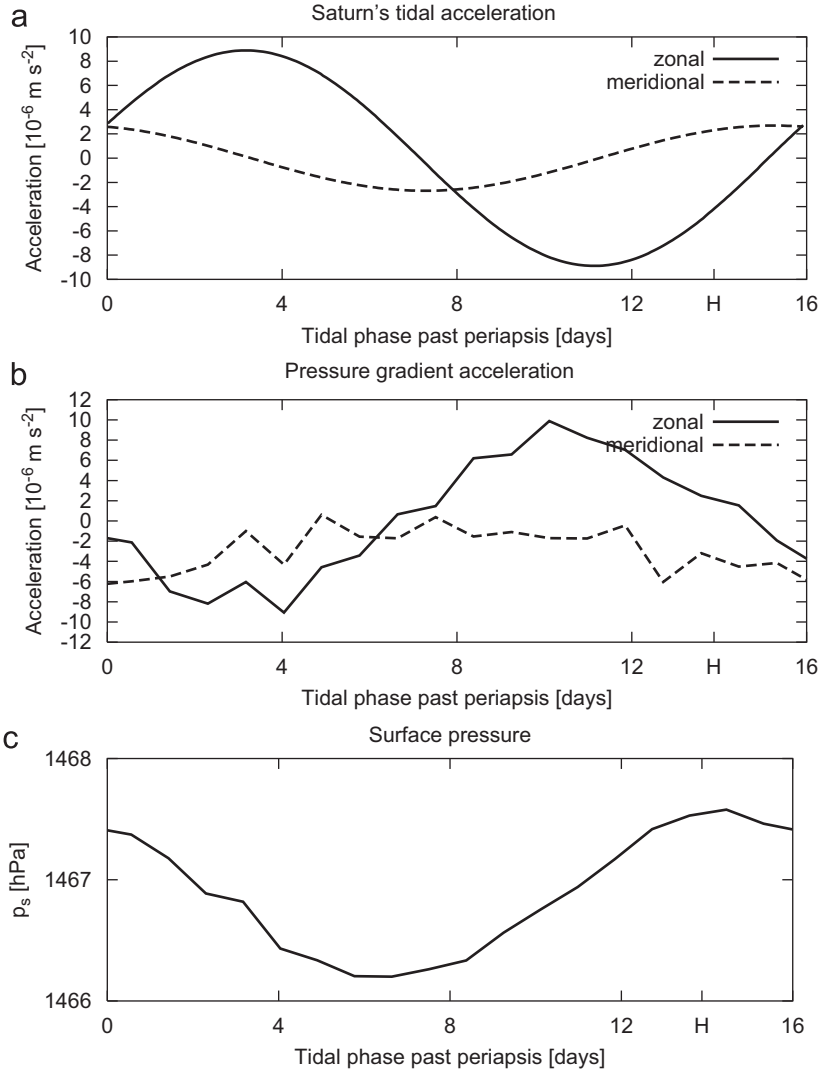

Fig. 10. (a) Diurnal variation in the zonal and meridional component of Saturn's gravitational tidal acceleration af the Huygens site (10°S, 168°E) calculated after Tokano and Neubauer (2002). At the time of Huygens descent the tide was northwestward, with a zonal component of $-4.1\times10^{-6}\,\mathrm{m\,s^{-2}}$ and a meridional component of $2.3\times10^{-6}\,\mathrm{m\,s^{-2}}$. At this near-equatorial site the zonal tide has a larger amplitude than the meridional one. The instantaneous global map of the tide is similar to that of day 14 in Fig. 2 of Tokano and Neubauer (2002). (b) Diurnal variation in the zonal and meridional pressure gradient acceleration at the Huygens site predicted by the GCM. (c) Diurnal variation in the surface pressure at the Huygens site predicted by the GCM. The time axis is expressed in terms of Titan's tidal phase in days beginning from periapsis (day 0), via apoapsis (day 8), the Huygens landing time (day 13.88) to the following periapsis (day 16) as defined in Tokano and Neubauer (2002).

summer and autumn (from $L_S = 270^\circ$ to shortly before $L_S = 90^\circ$), and southward wind otherwise. Below 1 km this is exactly reversed. At the Huygens season v is southward below 800 m and the maximum speed occurs near the surface. Above 800 m v turns to northward, with a nearly uniform speed of $0.05\,\mathrm{m\,s^{-1}}$ up to 7 km. Above 7 km v becomes negligible. This vertical profile is very consistent with the wind profile retrieved by Karkoschka et al. (2007). Both the altitude of the reversal as well as the fact that the near-surface v is faster than further above are well reproduced by the GCM. This seasonal pattern is likely to be related to the Hadley circulation and its seasonal reversal (Fig. 7) and the altitude of the reversal of the meridional wind direction corresponds to the core of the mass streamfunction.

The instantaneous meridional wind at the Huygens site (Fig. 6b) changes direction at several altitudes. Southward wind is found from the surface up to 3 km and between 8 and 16 km, while northward wind occurs in between. Remarkably, the southward wind is strongest in the PBL, with $-0.25\,\mathrm{m\,s^{-1}}$. This meridional wind reversal is mainly a result of the near-surface Hadley circulation whose core is located near 2 km (Fig. 7). The near-surface southward flow represents the lower branch of the Hadley cell beneath the core. The northward flow between 3 and 8 km is located in the upper branch of the Hadley cell, with a flow from the summer (south) to winter (north) hemisphere.

However, the southward flow above 8 km cannot be explained by the Hadley circulation alone, as the mass

streamfunction indicate mean northward flow all the way above 1 km (Fig. 7). Thus this is likely to reflect a transient feature not visible in the mean meridional circulation pattern. At this altitude the horizontal temperature gradient is already quite small (Fig. 4), so the pressure gradient associated with inhomogeneous temperature distribution is smaller than that caused by Saturn's gravitational tide. As the meridional component of the tide is northward (Fig. 10a) the pressure gradient force is southward (Fig. 10b) to balance the tide, which is responsible for the southward wind in the upper troposphere.

4.2. Influence of Saturn's tide or the lack of it (Simulation 2)

In this subsection the influence of Saturn's gravitational tide on the actual zonal wind profile at the Huygens site is pursued, as the tide is predicted to affect both the zonal and meridional wind (Tokano and Neubauer, 2002). To investigate the impact of the tide or the lack of it on the wind field the GCM run (with seasonal forcing) is now repeated without tide, i.e. the tidal acceleration in the momentum equation is artificially switched off (Simulation 2). Fig. 6 shows a comparison of the instantaneous vertical profile of zonal wind at the place and time of Huygens' landing predicted by the GCM with (Simulation 1) and without tide (Simulation 2). The zonal wind does not differ much from the simulation in which the tide is included. At least the influence of the tide on u is much smaller than the seasonal difference.

However, the zonal wind near the surface remains retrograde, while in Simulation 1 it reverses to slightly prograde near 500 m. In the absence of tide the instantaneous zonal wind is systematically shifted by $\sim -0.3\,\mathrm{m\,s^{-1}}$ in comparison with the simulation with tide. This small difference can only be ascribed to the absence of tide. If the tide is included, the westward tidal acceleration (Fig. 10a) gives rise to an eastward pressure gradient force at the time of Huygens' landing (Fig. 10b). Since the Coriolis force is negligible in the PBL the presence of an eastward pressure gradient force immediately causes eastward wind. If, on the other hand, the tide is absent, the longitudinal pressure gradient disappears and the zonal wind in the PBL is primarily affected by the vertical transport of angular momentum. Thus the zonal wind in the PBL is something between zero and the retrograde wind outside the PBL.

The right column of Figs. 8 and 9 shows the horizontal temperature and wind field at selected levels predicted in the absence of tide. The global temperature field barely differs from that in the presence of tide since the tide does not directly affect the thermally forced Hadley circulation. The major difference is found in the surface pressure field that lacks a clear longitudinal variation. The marked wave 2 pattern caused by the tide disappears, although some irregular fluctuations caused by the turbulence in the PBL remains. The wind field in the free atmosphere is mostly zonal and the meridional wind almost disappears. Also the vertical profile (Fig. 6b) reveals that the tide does not seem to systematically and substantially affect the meridional wind.

In the PBL, however, there are still substantial meridional winds although the global pattern does not agree with that predicted in the presence of tide. Generally southward flow in the equatorial regions exists even in the absence of tide (Fig. 9h), reinforcing that this is caused by the southward pressure decrease near the surface, i.e. by the lower branch of the cross-equatorial Hadley circulation. The slightly weaker southward wind in the PBL (Fig. 6b) in comparison with Simulation 1 may be explained by the lack of tide.

4.3. Influence of seasonality (Simulation 3)

The baseline simulation presented in Section 4.1 was run under ordinary seasonal variation in the solar forcing. However, another series of Titan GCM (Rannou et al., 2004, 2006) predicts more or less hemispherically symmetric surface temperature throughout the year. This could occur if there is a permanent accumulation of haze particles in the polar region of either hemisphere. In this case the seasonality ceases in the lower troposphere in that the latitudinal distribution of insolation becomes more or less symmetric about the equator throughout the year.

To account for this hypothetical effect we repeat the same Titan GCM simulation without seasonal variation in the insolation (Simulation 3). The solar declination is set to 0° during the entire simulation, so the equator always receives the largest amount of sunlight. The resulting global field of zonal wind and temperature is, not surprisingly, symmetric about the equator (Fig. 11c and d). In contrast to the simulation with seasonal variation the temperature monotonically decreases with latitude in either hemisphere up to about 5 km and the zonal wind is almost everywhere prograde, with stationary tropospheric jets near 50° latitude and 5 km altitude. The only exception to this is the PBL close to the surface. In other words regions with easterlies (retrograde wind) virtually disappear in this simulation. Most remarkably, the wind in the equatorial region is now prograde although the wind speed is very low.

The simultaneous formation and maintenance of westerlies in either hemisphere can be explained by the surface–atmosphere transfer of angular momentum by the easterlies near the surface and subsequent transport of it by the equator-to-pole equinox-type Hadley circulation. The decrease of the temperature with latitude implies positive thermal wind, i.e. the westerly zonal wind increases with altitude up to the level at which the latitudinal temperature gradient ceases (5 km). Above 5 km the zonal wind diminishes since there is a slight increase of the temperature with latitude. At the Huygens site the

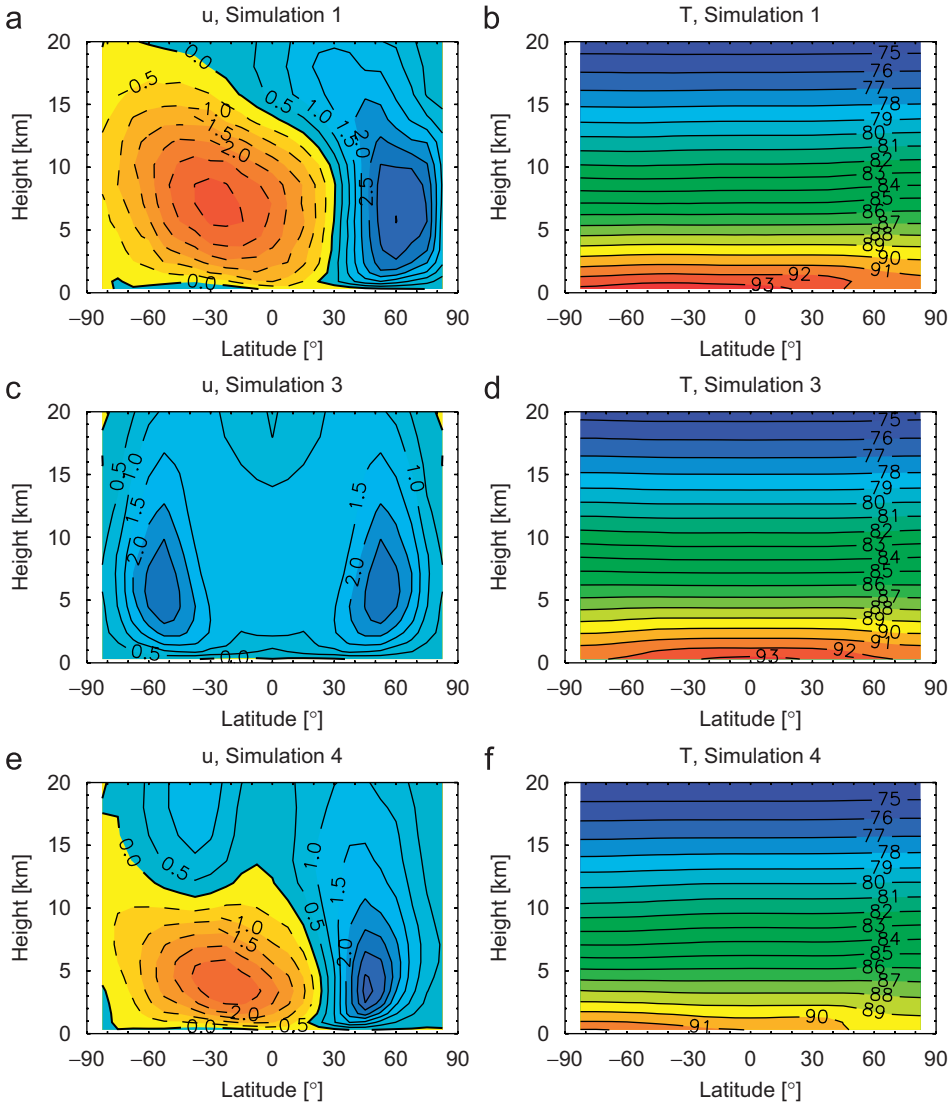

Fig. 11. Meridional–vertical cross-section of zonally and diurnally averaged zonal wind in $m\,s^{-1}$ (left column) and temperature in K (right column) in the Huygens season predicted under different conditions. The result of Simulation 2 is almost identical to that of Simulation 1, and thus is not shown.

predicted zonal wind is prograde in the entire troposphere, with wind speeds of $\sim 1\,m\,s^{-1}$ and little variation with height (Fig. 6). This profile is qualitatively inconsistent with the observation in that the reversal of the wind direction and the retrograde wind are absent.

Also Grieger et al. (2004) showed that in the absence of a hemispheric asymmetry in the tropospheric temperature the near-surface easterlies substantially weaken in comparison with a model version with a warmer summer pole. The GCM of Luz et al. (2003) and Rannou et al. (2004) predict that in the equatorial region the zonal wind is prograde almost everywhere except in the lowest 100 m or so. In their model the near-surface temperature is symmetric about the equator even in the Huygens season. We note that, in contrast to their present GCM version, their early 3D version of the GCM (Hourdin et al., 1995) did generate retrograde wind at the Huygens site from the surface up to about 1000 hPa (6 km). In that version the near-surface temperature at the solstice was asymmetric about the equator.

On the basis of this simulation and comparison with other GCMs we can conclude that on Titan easterlies preferentially develop in regions with a temperature increase with latitude down to the surface and the wind balance is closer to geostrophic than to cyclostrophic, as is the case in the lower troposphere. Seasonal variation in the surface and near-surface temperature contributes a major part in the generation of substantial easterlies in the lowest few kilometres. At the same time the presence of these easterlies is consistent with a warmer southern (summer) hemisphere compared with the equator in the Huygens season.

Fig. 7b shows the mass streamfunction of the Hadley circulation under the condition that no seasonality exists, i.e. under a permanent equinox condition. The tropospheric Hadley circulation in this case is split into four

cells. A thermally direct cell extends from the equator to 40° latitude in each hemisphere. Another, thermally indirect cell extends from there to the poles. In contrast to the baseline simulation there is no cross-equatorial mean flow any more and the mass flux is smaller by a factor of 5. A comparison of Fig. 7a and b clarifies that the mean meridional wind direction at the Huygens site (10°S) is opposite to that predicted in the baseline simulation, i.e. the near-surface flow is northward (equatorward), while at higher altitudes the mean flow is poleward (southward). This meridional circulation pattern shows some resemblance to that predicted by Rannou et al. (2006) in that several cells are located side by side. However, oblique cells as predicted by Rannou et al. (2006) are not predicted in the present model and this may be the influence of tropospheric methane clouds not simulated here.

These differences to the baseline simulation can also be recognised in the instantaneous vertical profile of v at the Huygens site (Fig. 6b). The meridional wind barely exceeds 0.1 m s^{-1} although the tide is taken into account in the simulation. Persistent northward wind between 7 km and 800 m as well as the southward wind below that level observed by DISR are not reproduced at all. This reflects the lack of a cross-equatorial temperature and pressure gradient in this scenario.

4.4. Sensitivity to the heating rate (Simulation 4)

Another parameter that requires attention in the context of this study is the strength of the Hadley circulation, which not only represents the meridional wind, but also affects the zonal wind profile by virtue of global redistribution of angular momentum. Zhu and Strobel (2005) found in a sensitivity experiment with a two-dimensional model of Titan's stratosphere that the strength of the meridional circulation directly scales with the radiative forcing. If in their model the radiative heating rate was increased by a factor of 10, the meridional circulation increased by the same factor, too. The GCM of Rannou et al. (2004) is another example that shows how the radiative flux affects the meridional circulation. In comparison with previous simulations with a fixed haze distribution the meridional circulation in the stratosphere was intensified. However, since both Rannou et al. (2004) and Zhu and Strobel (2005) focussed on the stratosphere it is not evident from their studies how the change in the radiative forcing affects the meridional and zonal circulation in the troposphere.

The net heating rate is the sum of solar heating rate and thermal cooling rate, and is the driving force of the Hadley circulation. In the lower 20 km the solar heating rate at the Huygens site predicted by the GCM is 2×10^{-8} K s^{-1} or less, and increases slowly with altitude. The amount of the thermal cooling rate is less than 10^{-8} K s^{-1}, thus smaller than the solar heating rate, so the net heating rate is larger, as expected for the equatorial region. Near the surface the temperature at the Huygens site (Fig. 12) closely matches

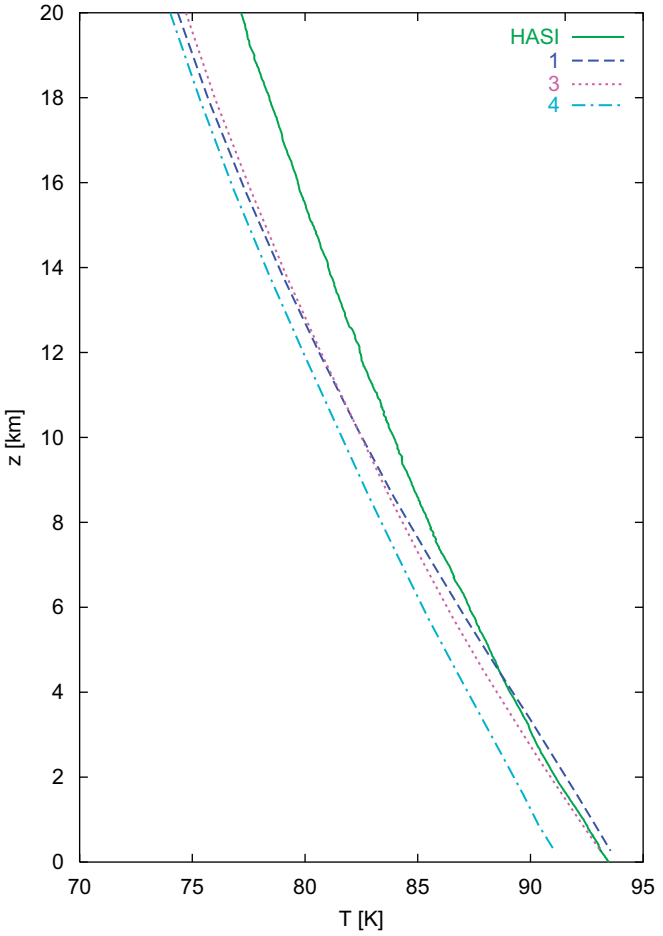

Fig. 12. Instantaneous vertical profile of temperature at the Huygens site at the time of landing predicted by the GCM under different conditions. The numbers denote the simulation number listed in Table 1. The temperature measured by HASI (Fulchignoni et al., 2005) is shown for comparison. The result of Simulation 2 is almost identical to that of Simulation 1, and thus is not shown.

the temperature measured by HASI (Fulchignoni et al., 2005), but with increasing altitude the predicted temperature shows a negative deviation. This indicates that either the solar heating rate is underestimated or the cooling rate is overestimated in the upper troposphere compared with the lower troposphere. However, it could also indicate that the vertical mixing of heat is excessive, so the lapse rate is closer to adiabatic than the measured lapse rate.

The calculation of the radiative heating rate in this GCM is based on the radiation model of McKay et al. (1989). The column optical depth in the visible spectrum varies between 2 and 2.5 and the troposphere was assumed to be clear of haze. However, Huygens detected that there is significant haze opacity at all altitudes down to the surface (Tomasko et al., 2005). The measured column optical depth of the haze is 4–5 at 531 nm and 2.5–3.5 at 329 nm. This indicates that a smaller amount of sunlight should arrive at Titan's surface and the solar heating rate in the lower troposphere may be smaller than predicted by the

GCM, while a larger amount of solar radiation may be absorbed at higher altitudes.

Given this fact, we reduce in Simulation 4 the solar heating rate intentionally by a factor of 2 with respect to the baseline simulation. While this ad hoc assumption is simplistic, future studies taking into account detailed results of the Huygens DISR concerning the radiative budget in Titan's atmosphere may constrain the radiative forcing relevant in GCMs.

This modification introduces several quantitative changes in the lower troposphere. First the temperature drops by up to 2 K compared with the baseline simulation (Fig. 12). The temperature decrease is most pronounced near the surface. The predicted temperature does not fit the HASI temperature profile at any altitude. On the other hand the predicted lapse rate, which is smaller than in the baseline simulation, agrees much better with that observed by HASI. This suggests that at least the convective heat transport may be more realistically reproduced in the model.

Another consequence of the reduced solar heating is the weakening of the tropospheric Hadley circulation while the circulation pattern does not change (Fig. 7). Compared with the baseline simulation the mass streamfunction reduces by up to a factor of 2 in the lower troposphere. This also means that the amount of angular momentum transported from one hemisphere to another on seasonal timescales becomes smaller and the hemispherical asymmetry is somewhat less pronounced. While the zonal wind in the lower troposphere still exhibits a pair of prograde and retrograde jet (Fig. 11e), both of them are weaker. Also the retrograde wind of the summer hemisphere does not extend as high as in the baseline simulation.

The instantaneous zonal wind at the Huygens site (Fig. 6a) in the lower 5 km closely follows that in the baseline simulation. Maximum retrograde wind occurs near 5 km and above this level the wind speed decreases and turns to prograde wind by 12 km. In other words, the wind reversal takes place at a lower altitude than in the baseline simulation although this is still higher than observed. Also the predicted maximum retrograde wind near 5 km is much sharper and thus resembles that observed by the Huygens DWE (Folkner et al., 2006). This change can be ascribed to the different magnitudes of the seasonal angular momentum transport and it seems that an even slightly weaker interhemispherical Hadley circulation could generate the observed wind profile. However, the underestimated wind speed in the upper troposphere can probably not be readily generated by a further simple modification of the Hadley circulation pattern, as this bias is common to all simulations presented here. Perhaps the radiative heating pattern at higher altitudes would have to be reevaluated based, e.g. on information from Huygens. Nevertheless, this sensitivity study indicates that a change in the radiative heating profile in the troposphere can shift the altitude of the zonal wind reversal to some extent.

5. Descent trajectory simulation

An alternative way of verifying the vertical profile of wind speed and direction with the Huygens data is to compare the descent trajectory of the probe with that calculated with the predicted zonal and meridional wind. The descent trajectory was reconstructed by the Huygens DISR by visual ground tracking of the probe (Tomasko et al., 2005; Karkoschka et al., 2007), as also mentioned in Section 2.

The descent trajectory of the probe can be calculated as

$$\mathbf{X}(t+\Delta t) = \mathbf{X}(t) + (u, v, w)(t)\Delta t, \quad (4)$$

where $\mathbf{X}$ is the instantaneous three-dimensional cartesian coordinate of the probe, $\Delta t = 5$ s is the time step interval and (u, v, w) is the zonal, meridional and vertical drift speed of the probe. It is assumed that the probe movement immediately responds to the instantaneous wind speed since the response time of Huygens was merely 3–5 s in the lowest 10 km (Bird et al., 2005), thus comparable with the time step interval in this calculation. Here, the instantaneous values of u and v predicted by the GCM for the Huygens site as a function of altitude are used. w is the probe's descent speed that was reconstructed from the temperature and pressure profile measured by HASI (Harri et al., 2006). The simulation is started at an altitude of 20 km and for the sake of a convenient comparison with the observed trajectory (Karkoschka et al., 2007), the coordinate is centred at the respective predicted landing point. Here, the x- and y-axis correspond to Titan's east longitude and latitude.

Figs. 13a and b depict the calculated descent trajectory projected on the surface using the predicted vertical profile of zonal and meridional wind with a different zoom. In the baseline simulation (Simulation 1) the probe mostly drifts westward after an initial clockwise loop near 20 km. There is an additional slight meridional drift, which is initially southward and then turns to northward. The initial westward drift is clearly inconsistent with observation (Karkoschka et al., 2007), confirming the wrong predicted altitude of the zonal wind reversal. Furthermore, in comparison with the observation, the predicted northward drift below 7 km is underestimated by a factor of about 2. This may indicate that the predicted meridional flow in the upper branch of the Hadley cell is too low.

Remarkably, the model predicts a sharp left turn by more than 90° near 800 m altitude. Eventually the probe approaches the surface towards southeast to south-southeast. While this is dissimilar to an Earth-like Ekman spiral, the last portion of the trajectory almost exactly fits the observational data (Fig. 13b). Therefore, the lower branch of the Hadley cell and/or the near-surface tidal wind seems to be realistically reproduced. The GCM does not resolve the PBL below 300 m, but since also the

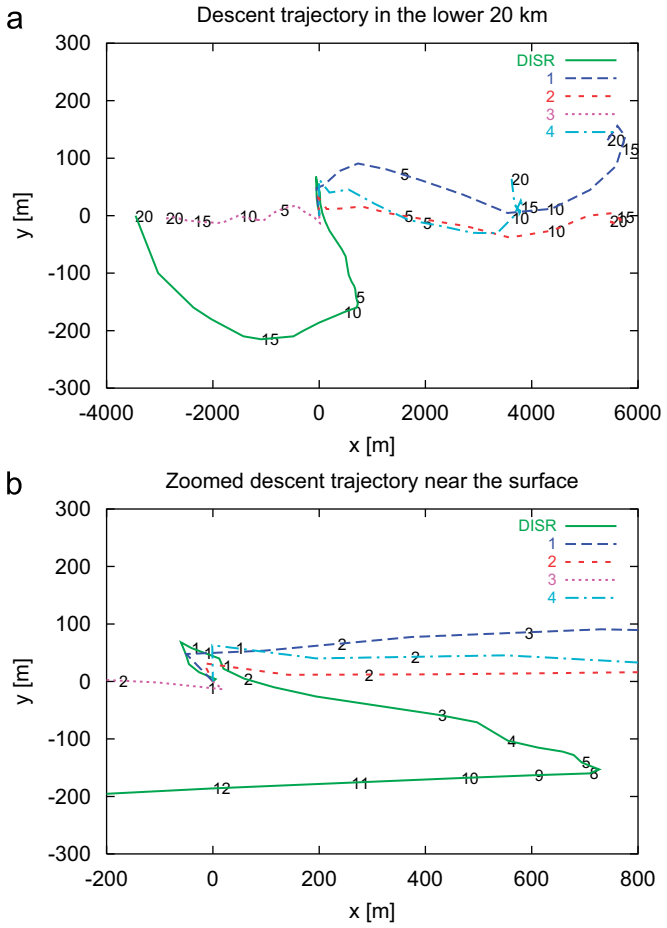

Fig. 13. Simulated descent trajectories of the Huygens probe using the predicted horizontal wind speed and the measured probe descent speed starting from an altitude of 20 km. Each trajectory is centred at the predicted landing site, where the x- and y-axis correspond to Titan's longitude and latitude, respectively. The descent trajectory observed by the Huygens DISR (Karkoschka et al., 2007) is also shown for comparison. Panel (a) shows the entire domain, but the x- and y-axis are not in scale considering the larger longitudinal drift compared with the meridional drift. Panel (b) shows the zoom of the landing site and the x- and y-axis are in scale. The numbers on each trajectory mark the altitude and the numbers on the margin denote the simulation numbers listed in Table 1.

Huygens probe could not directly constrain the probe drift below 250 m for technical reasons (Karkoschka et al., 2007) we do not pursue the detailed wind profile below 300 m.

The error in the predicted trajectory arising from the assumption of an instantaneous response of the probe drift to the change in wind speed is negligible in the lower part of the troposphere. With a descent speed of less than 7 m s^{-1} (Harri et al., 2006), the vertical distance traversed during the 3–5 s response time is about 30 m, and the predicted and observed vertical shear of the wind speed in this vertical interval is only 7.5×10^{-3} m s^{-1}. If a response time of 5 s is taken into account in the descent trajectory simulation, the predicted landing point shifts only by a few metres, so it was not plotted in the figure.

Simulation 2, which excludes Saturn's tide, generates a slightly different descent trajectory. The probe performs a westward drift almost without additional meridional drift. Hence Saturn's tidal force indeed seems to enhance the overall meridional wind. Below 800 m the probe turns to the left, as in Simulation 1, but the southeastward drift is smaller than in the presence of tide and less consistent with observation. Since the only difference between Simulation 1 and 2 is the presence or absence of tide the slightly better agreement of the trajectory of Simulation 1 with the DISR data may be interpreted as a result of Saturn's gravitational tide.

The descent trajectory in Simulation 3 (without seasonality) is more inconsistent with the Huygens data than Simulations 1 and 2 because the predicted drift of the probe is almost only eastward. Exceptionally, the drift in the final portion of the descent below 1 km is northwestward, but this is also opposite to what was observed by DISR. This discrepancy indicates that the presence of an equinox-type Hadley cell with an equatorward flow near the surface and a poleward flow above it is unlikely to have existed at the time of Huygens' landing.

The result of Simulation 4 (reduced heating rate) is rather similar to that of Simulation 1 below 10 km, but the westward drift is smaller and thus more consistent with the DISR data. The sharp left turn near 800 m is predicted as well, although the eastward component is slightly weaker than in Simulation 1. The anti-clockwise spiral in the highest part of the descent goes in the opposite sense from Simulation 1, but this sense is more consistent with the DISR data than the clockwise turn of Simulation 1 although the observed spiral is not as narrow as predicted. However, the predicted southward drift direction in the final portion of the descent below 1 km deviates from the observed one by 45°.

While the reduction of the diabatic heating rate certainly weakens the Hadley circulation, this does not simply cause a slower meridional wind speed, but also changes the vertical profile of zonal wind and the actual force balance at each altitude, as described in the previous section, so the prediction of the expected change in the descent trajectory is not straightforward, as illustrated in this simulation.

As a whole none of the simulated descent trajectory can exactly fit the observed descent trajectory, but the combination of the northwestward drift below 7 km and the southeastward drift below 800 m is better reproduced by Simulation 1 than in other simulations. This means that a combination of seasonally varying Hadley circulation with a cross-equatorial southward temperature increases near the surface at the time of landing and Saturn's gravitational tide may substantially contribute to the observed wind profile.

It is evident that the descent trajectory is sensitive to various factors in the troposphere such as tide, seasonal variation or solar heating rate. Although not explicitly simulated in this study it is also likely that other factors such as surface properties including topography or clouds would also affect the near-surface wind profile. Therefore, it is a formidable task to simultaneously tune the

parameters such as to exactly fit the zonal and meridional wind as well as temperature.

6. Discussion and conclusions

This study has shown in some detail how sensitively the wind near the surface depends on various forces as well as how the zonal and meridional wind depend on each other. The observed wind profile does not resemble characteristic wind profiles of the terrestrial PBL such as an Ekman spiral of a neutrally stratified PBL, a uniform wind profile characteristic of a strongly convective PBL or a low-level jet typical for the nocturnal PBL. Instead the global-scale atmospheric dynamics seems to control the actual wind profile.

Unlike in the stratosphere, which is characterised by super-rotating prograde winds in either hemisphere (Bird et al., 2005; Flasar et al., 2005; Luz et al., 2005; Kostiuk et al., 2006), this GCM suggests that the zonal wind direction in the lower troposphere varies with season. This occurs because the cyclostrophic wind balance breaks down near Titan's surface and thus the hemispheric asymmetry in the temperature field gives rise to a global Hadley circulation that transport angular momentum from one hemisphere to the other. As a consequence, prograde and retrograde wind arise, depending on whether the temperature decreases or increases with latitude. The detected substantial retrograde winds in the lowest few kilometres of the Huygens site are consistent with this mechanism, and may be contrasted to the lower atmosphere of Venus that lacks a reversal of the zonal wind direction and substantial seasonality (Gierasch et al., 1998). The simulation shows that, if there were no seasonal variation in the tropospheric temperature and Hadley circulation pattern, the equatorial wind would have been prograde down to very close to the surface. Thus one major difference between Venus and Titan, both representing slowly rotating planetary bodies with a thick atmosphere, is the impact of seasonal variation on the zonal wind.

The meridional wind at the Huygens site is mainly a manifestation of the cross-equatorial Hadley circulation. While immediately above the surface the meridional flow is southward following the southward pressure gradient force and representing the lower branch of the Hadley circulation, a reversed flow is found above 1 km, representing the upper branch of the Hadley circulation. The altitude of the zonal and meridional wind reversal should depend on up to which the altitude seasonal variation in temperature induced by the sensible heat flux from the surface can be felt. The occurrence of the wind reversal between 7 and 10 km (Karkoschka et al., 2007) indicates that the horizontal temperature gradient may change sign a few km below this altitude.

Another wind reversal closer to the surface (800 m) indicates a transition between two regimes with different force balances. Below 800 m the major force balance is that between Saturn's gravitational tide and pressure gradient force. Above 800 m the major force balance is that between the pressure gradient force, Coriolis force and Saturn's gravitational tide. The cyclostrophic balance relevant in the stratosphere is negligible in the lower troposphere anyway.

The influence of Saturn's tide is rather small at the Huygens site given its proximity to the symmetry axis of the tide, i.e. the equator. While the zonal and meridional wind do not exhibit a clear signature of tidal wind, the southeastward wind near the surface can be generated in the presence of tide.

However, it should be noted that the near-surface wind direction is likely to be modified by local topography, as pointed by Lorenz et al. (2006) after examining the orientation of sand dunes. For this reason a firm conclusion about the significance of the tidal wind on the basis of the single measurement by Huygens is difficult.

The result of this model study has several implications for Titan's tropospheric meteorology and geophysics. First, this study suggests the likelihood of a warmer southern (summer) hemisphere in comparison with the equator. If so, this would favour the insolation hypothesis for the generation of convective clouds (Brown et al., 2002; Tokano, 2005; Schaller et al., 2006). Secondly, the seasonal reversal of the tropospheric Hadley circulation implies that some exchange of angular momentum is likely to occur on seasonal timescales between the surface and atmosphere, with a possible impact on a seasonal variation in Titan's length-of-day (Tokano and Neubauer, 2005).

The simulation also indicates that the temporal variation in both the zonal and meridional wind in the lower troposphere largely depends on the strength of the seasonal temperature variation and Hadley circulation. Thus, the strength of the seasonality in Titan's troposphere may depend on how much sunlight penetrates to Titan's surface and how asymmetric the surface temperature becomes at solstice. The incorrect prediction of the altitude of the zonal wind reversal is likely to reflect inaccuracies in the GCM in calculating the radiative fluxes and thus of inaccurate reproduction of the Hadley circulation or temperature. In situ data on the properties of atmospheric opacity sources or radiative fluxes at the Huygens site currently under analysis by the Huygens teams can probably improve these details of the GCM in the near future. In addition, possible future balloon missions to Titan would further constrain the wind system in Titan's lower troposphere (Tokano and Lorenz, 2006).

Acknowledgements

The author received a grant from the DFG (Deutsche Forschungsgemeinschaft) in the priority programme "Mars and the Terrestrial Planets". He is also grateful for Björn Grieger and an anonymous reviewer for constructive suggestions. The Java program Titan24 (available at http://www.giss.nasa.gov/tools/titan24) was used to calculate the astronomical parameters used in this study.

References

Bird, M.K., et al., 2005. The vertical profile of winds on Titan. Nature 43, 800–802.

Bouchez, A.H., Brown, M.E., 2005. Statistics of Titan's south polar tropospheric clouds. Astrophys. J. 618, L53–L56.

Brown, M.E., Bouchez, A.H., Griffith, C.A., 2002. Direct detection of variable tropospheric clouds near Titan's south pole. Nature 420, 795–797.

Flasar, F.M., et al., 2005. Titan's atmospheric temperatures, winds, and composition. Science 308, 975–978.

Folkner, W.M., Asmar, S.W., Border, J.S., Franklin, G.W., Finley, S.G., Gorelik, J., Johnston, D.V., Kerzhanovich, V.V., Lowe, S.T., Preston, R.A., Bird, M.K., Dutta-Roy, R., Allison, M., Atkinson, D.H., Edenhofer, P., Plettemeier, D., Tyler, G.L., 2006. Winds on Titan from ground-based tracking of the Huygens probe. J. Geophys. Res. 111, E07S02.

Fulchignoni, M., et al., 2005. *In situ* measurements of the physical characteristics of Titan's environment. Nature 438, 785–791.

Gierasch, P.J., et al., 1998. The general circulation of the Venus atmosphere: an assessment. In: Bougher, S.W., Hunten, D.M., Phillips, R.J., et al. (Eds.), Venus II. University of Arizona Press, Tucson, pp. 459–500.

Grieger, B., Segschneider, J., Keller, H.U., Rodin, A.V., Lunkeit, F., Kirk, E., Fraedrich, K., 2004. Simulating Titan's tropospheric circulation with the portable university model of the atmosphere. Adv. Space Res. 34, 1650–1654.

Griffith, C.A., Penteado, P., Baines, K., Drossart, P., Barnes, J., Bellucci, G., Bibring, J., Brown, R., Buratti, B., Capaccioni, F., Cerroni, P., Clark, R., Combes, M., Coradini, A., Cruikshank, D., Formisano, V., Jaumann, R., Langevin, Y., Matson, D., McCord, T., Mennella, V., Nelson, R., Nicholson, P., Sicardy, B., Sotin, C., Soderblom, L.A., Kursinksi, R., 2005. The evolution of Titan's mid-latitude clouds. Science 310, 474–477.

Harri, A.-M., Mäkinen, T., Lehto, A., Kahanpää, H., Siili, T., 2006. Vertical pressure profile of Titan—observations of the PPI/HASI instrument. Planet. Space Sci. 54, 1117–1123.

Hourdin, F., Talagrand, O., Sadourny, R., Courtin, R., Gautier, D., McKay, C.P., 1995. Numerical simulation of the general circulation of the atmosphere of Titan. Icarus 117, 358–374.

Karkoschka, E., Tomasko, M.G., Doose, L.R., Rizk, B., See, C., McFarlane, L., Schröder, S., 2007. DISR imaging and the geometry of the descent of the Huygens probe within Titan's atmosphere. Planet. Space Sci., in press, doi:10.1016/j.pss.2007.04.019.

Kostiuk, T., Livengood, T.A., Sonnabend, G., Fast, K.E., Hewagama, T., Murakawa, K., Tokunaga, A.T., Annen, J., Buhl, D., Schmülling, F., Luz, D., Witasse, O., 2006. Stratospheric global winds on Titan at the time of Huygens descent. J. Geophys. Res. 111, E07S03.

Lellouch, E., Coustenis, A., Gautier, D., Raulin, F., Dubouloz, N., Frère, C., 1989. Titan's atmosphere and hypothesized ocean: a reanalysis of the Voyager 1 radio-occultation and IRIS 7. 7-μm data. Icarus 79, 328–349.

Lorenz, R.D., 2006. Thermal interactions of the Huygens probe with the Titan environment: constraint on near-surface wind. Icarus 182, 559–566.

Lorenz, R.D., et al., 2006. The sand seas of Titan: Cassini RADAR observations of longitudinal dunes. Science 312, 724–727.

Luz, D., Hourdin, F., Rannou, P., Lebonnois, S., 2003. Latitudinal transport of barotropic waves in Titan's stratosphere. II. Results from a coupled dynamics–microphysics–photochemistry GCM. Icarus 166, 343–358.

Luz, D., Civeit, T., Courtin, R., Lebreton, J.-P., Gautier, D., Rannou, P., Kaufer, A., Witasse, O., Lara, L., Ferri, F., 2005. Characterization of zonal winds in the stratosphere of Titan with UVES. Icarus 179, 497–510.

McKay, C.P., Pollack, J.B., Courtin, R., 1989. The thermal structure of Titan's atmosphere. Icarus 80, 23–53.

Niemann, H.B., et al., 2005. The abundances of constituents of Titan's atmosphere from the GCMS instrument on the Huygens probe. Nature 438, 779–784.

Porco, C.C., et al., 2005. Imaging of Titan from the Cassini spacecraft. Nature 434, 159–168.

Rannou, P., Hourdin, F., McKay, C.P., Luz, D., 2004. A coupled dynamics–microphysics model of Titan's atmosphere. Icarus 170, 443–462.

Rannou, P., Montmessin, F., Hourdin, F., Lebonnois, S., 2006. The latitudinal distribution of clouds on Titan. Science 311, 201–205.

Roe, H.G., Brown, M.E., Schaller, E.L., Bouchez, A.H., Trujillo, C.A., 2005. Geographic control of Titan's mid-latitude clouds. Science 310, 477–479.

Schaller, E.L., Brown, M.E., Roe, H.G., Bouchez, A.H., 2006. A large cloud outburst at Titan's south pole. Icarus 182, 224–229.

Stull, R.B., 1988. Introduction to Boundary Layer Meteorology. Kluwer Academic Publishers, Dordrecht.

Tokano, T., 2005. Meteorological assessment of the surface temperatures on Titan: constraints on the surface type. Icarus 173, 222–242.

Tokano, T., Lorenz, R.D., 2006. GCM simulation of balloon trajectories on Titan. Planet. Space Sci. 54, 685–694.

Tokano, T., Neubauer, F.M., 2002. Tidal winds on Titan caused by Saturn. Icarus 158, 499–515.

Tokano, T., Neubauer, F.M., 2005. Wind-induced seasonal angular momentum exchange at Titan's surface and its influence on Titan's length-of-day. Geophys. Res. Lett. 32, L24203.

Tokano, T., Neubauer, F.M., Laube, M., McKay, C.P., 1999. Seasonal variation of Titan's atmospheric structure simulated by a general circulation model. Planet. Space Sci. 47, 493–520.

Tokano, T., Ferri, F., Colombatti, G., Mäkinen, T., Fulchignoni, M., 2006. Titan's planetary boundary layer structure at the Huygens landing site. J. Geophys. Res. 111, E08007.

Tokano, T., Neubauer, F.M., Laube, M., McKay, C.P., 2001. Three-dimensional modeling of the tropospheric methane cycle on Titan. Icarus 153, 130–147.

Tomasko, M.G., et al., 2005. Rain, winds and haze during the Huygens probe's descent to Titan's surface. Nature 438, 765–778.

Zhu, X., Strobel, D.F., 2005. On the maintenance of thermal wind balance and equatorial superrotation in Titan's stratosphere. Icarus 176, 331–350.